Room-Temperature Molecular Manipulation via Plasmonic Trapping at Electrified Interfaces

*Nobuaki Oyamada, Hiro Minamimoto, and Kei Murakoshi**

Department of Chemistry, Faculty of Science, Hokkaido University, Sapporo, Hokkaido 060-0810, Japan.

kei@sci.hokudai.ac.jp

KEYWORD.

Optical Force, Plasmon Resonance, Surface-Enhanced Raman Scattering, Electrochemical Potential Control, Bi-Analyte Method

ABSTRACT

For the motion control of individual molecules at room temperature, optical tweezers could be one of the best approaches to realize desirable selectivity with high resolution in time and space. Because of physical limitations due to the thermal fluctuation, optical manipulation of small molecules at room temperature is still a challenging subject. The difficulty of the manipulation also emerged from the variation of molecular polarizability depending on the choice of molecules as well as the molecular orientation to the optical field. In this article, we have demonstrated plasmonic optical trapping of small size molecules with less than 1 nm at

the gap of a single metal nanodimer immersed in an electrolyte solution. In situ electrochemical surface-enhanced Raman scattering measurements prove that a plasmonic structure under electrochemical potential control realizes not only the selective molecular condensation but also the formation of unique mixed molecular phases which is distinct from those under a thermodynamic equilibrium. Through detailed analyses of optical trapping behavior, we established the methodology of plasmonic optical trapping to create the novel adsorption isotherm under applying an optical force at electrified interfaces.

INTRODUCTION

The enhancement of the light-molecular interaction could open various possibilities of the novel applications at photoscience for energy conversion, ultra-sensitive detection, and material manipulation. The excitation of localized surface plasmon resonance (LSPR) at the metal nanostructures, leading to the formation of the localized strong electric field, can improve the light-molecular responses. LSPR is the collective oscillation of the free electrons in the metal nanostructures triggered by the visible light illumination. Thus, optical properties of metal nanostructures are precisely tuned by the control of their sizes, shapes, or metal species.[1,2] For example, the bowtie structure with the gap distance of less than 5 nm generates the relatively strong optical field (hot spot) at the gap.[3–5] Within such plasmonic field, various unique photo response phenomena, *e.g.* the formation of the new hybridized state, the enhancement of Raman scattering, or efficient photochemical reactions, can be induced.[6–10] Our previous works have revealed that the selection rule of the electronic excitation is modified by the strong localization of the light field, leading to the formation of the novel excited states which are not produced by the normal light illumination.[11–15] In addition, very recently, we have found that the unique molecular selective condensation was observed at the hot spots

under the condition of the resonant electronic excitation at electrified interface.[16] This molecular condensation would be resulted from the improvement of the light-molecular interaction under the resonant condition.

It is well known that the focused light could manipulate small materials. This technique is recognized as the laser trapping which has the potential for the ultimate manipulation of chemicals.[2,17–22] The optical force (F_{opt}) under the laser light illumination can be described as follows.[17,23,24]

$$< \boldsymbol{F_{opt}} > = \frac{I_0 \mathrm{n}}{\varepsilon_0 \mathrm{c}} \{\alpha' \nabla \left(\frac{|\boldsymbol{E_{loc}}|}{|\boldsymbol{E_0}|}\right)^2 + \alpha'' \boldsymbol{k} \left(\frac{|\boldsymbol{E_{loc}}|}{|\boldsymbol{E_0}|}\right)^2\} \quad \text{(eq. 1)}$$

where n, ε_0, c, I_0, E_{loc}, and E_0 are the refractive index of the surrounding media, permittivity, the velocity of the light, incident light intensity, the intensity of the localized electric field, and the intensity of the electric field for the far field, respectively. The $\alpha'$and α'' are the real and imaginary polarizabilities of the targets. The former and latter parts of the right side of the eq. 1 indicate the gradient and dispersion forces, respectively. The strong gradient force results in the efficient light-induced trapping. Generally, the efficient trapping by the focused laser is limited to the micrometer scale-materials. This is because that the relatively small polarizability of the small size materials and the diffraction limit of the light prevent the F_{opt} to overcome the Brownian motion (~$k_B T$).[25–27] However, because the metal nanostructures can enhance the E_{loc} up to 1000 times under the plasmon excitation, the strong light (~10 mW cm^{-2}) illuminations onto the material at the hot spot can achieve the relatively strong F_{opt} (~ 0.1 pN (= optical potential of 1 $k_B T$ (4.1 $\times$ 10^{-21} J at 298 K)).[24] In fact, recent efforts demonstrate the trapping of relatively small materials, such as metal particles,[28,29] polystyrene beads,[26,30,31] protein,[32,33] dye molecules,[34,35] or quantum dots[36,37], at the plasmonic field. It is emphasized here that the target materials should still have the larger size or polarizability than 50 nm and ~2.0 $\times$ 10^{-38} C^2 m J^{-1}, respectively. [29] However, the several small size molecules, e.g. Rhodamin-6G, Crystal

Violet, or other fluorescent molecules, have been applied to the molecular trapping because they show the improved α' under the resonant condition, leading to ten times larger than that under the non-resonant condition.[24,38] Because of these facts, it can be said that the plasmon induced optical manipulation of small size molecules is still a big challenge.

As the evaluation tool for the plasmon-induced optical trapping, surface enhanced Raman scattering (SERS) can be applicated to observe molecular condensations due to its high resolution.[39–42] In this article, we report the results about the observations of the suppression of the molecular diffusion and formation of the unique condensed phase within the plasmonic field immersed in the bi-analyte aqueous solution of 4,4'-bipyridine (44bpy) and 2,2'-bipyridine (22bpy). In our previous study, we have observed the evolution of resonant state of 44bpy depending on the molecule orientation, which is expected for the increment in the optical force.[16,43] To evaluate the molecular manipulations induced by the optical force at the plasmonic field, SERS measurements have been conducted under the electrochemical potential control. Electrochemical method makes it possible to control not only the orientation of molecules adsorbed onto the metal surface but also the resonance state of molecules as we reported before.[16] Thus, *in-situ* electrochemical SERS observations directly allow us to distinguish the adsorbing species, amount, configuration, and interaction among molecules.[42,44] The results strongly support the occurrence of the molecular selective manipulation leading to the formation of the novel condensed state which cannot be obtained under the normal condition. As the important point for the current achievements, we have proved that the unique interaction between adsorbing molecules under the optical manipulation can help to realize the behaviors of the small size molecule condensation

EXPERIMENTAL SECTION

Preparation of plasmonic structures

For *in-situ* electrochemical SERS measurements of plasmon induced optical manipulation, a plasmonic structures were prepared on the conductive by electron beam drawing at the Open Facility, Global Facility Center, Creative Research Institution, Hokkaido University.[45] After spin-coating a resist solution (ZEP520A: ZEPA = 2: 1) on the cleaned indium tin oxide (ITO) glass surface, it was heated at 140 °C for 3 min. The electron beam lithography has been performed with electron source scanning electron microscopy (ELS-F125: Elionix) with the applied voltage of 125 kV and the current of 50 pA under less than 10^{-4} Pa. The design for electron beam irradiation was same as that in our previous paper but triangles are made with three types: 100 nm × 120 nm for Fig 2 and Fig.3, 100 nm×150 nm for Fig. 4, and 100 nm×200 nm for Fig. 5 in here.[16] After electron beam irradiations, substrates were immersed in ZED-N50 for 60 sec and rinsed in ZMD-B for 10 sec. Using a sputtering machine (PMS-4000C1/HC1: ULVAC), 30 nm Au layer were deposited on an ITO surface and the resist layer after the deposition of 3 nm Ti layer as the adhesive layer. Then, the resist layer was removed in ZDMAC solution for 3 min and sonicating for 10 sec, afterwards, substrates was cleaned in acetone and methanol each for 10 sec. The prepared Au structures were examined by scanning electron microscopy (ELS-F125: Elionix).

Electrochemical SERS measurements

For evaluating molecular dynamics, electrochemical SERS measurements have been conducted using a home-made three electrodes electrochemical Raman cell as shown in Fig. 1a, the three electrode electrochemical cell was composed of Au bowtie / Ti / ITO substrate, Pt wire, and Ag / AgCl electrodes as the working electrode and counter electrode, and a reference electrode, respectively.[46] Electrochemical potential of the Au-bowtie structures were controlled by a potentiostat (HZ-5000: Hokuto Denko). The electrolyte solution was 0.1 M $NaClO_4$ aq. containing 4,4'-bipyridine (44bpy) and / or 2,2'-bipyridine (22bpy). The

concentrations of 44bpy and 22bpy were set to 1 μM or 1 mM. Raman spectra were collected by the 785 nm laser polarized parallel to the long axis of the bowtie structures. The significantly enhanced electric field strength at the gap is given only when a liner polarized light illuminates with parallel direction of long axis.[4,16,34] In addition, since there is such single structure in the laser west of incident light, it is thought that all SERS signal is originated from one hot spot in gap. All experiments were conducted under the ambient condition.

RESULTS AND DISCUSSION

The electrochemical SERS measurements have been performed using a three-electrode cell and the confocal Raman microscope system with the incident laser of λ_{ex} = 785 nm as illustrated in Fig. 1a and S1a. The plat form of the SERS substrate was the Au-bowtie which has the LSPR energy at around 785 nm depending on the polarized direction of the incident light. The calculated absorption/scattering spectra were provided in Fig. S1c. At the present study, we have used the structural isomers of bipyridine molecules (44bpy and 22bpy) which are shown in Fig. 1b. Theoretically estimated values of the polarizability depending on the molecular orientations are also shown. These estimated values are comparable to those in previous report.[47] Typical SERS spectra of 44bpy and 22bpy obtained from the single hot spot at the gap of bowtie structure (Fig. S1b) kept with a constant potential of −0.8 V are shown in the upper part of Fig. 1c and d, respectively. In the present electrochemical potential range, both bpy molecules are electrochemically stable without any redox reactions. The Raman band at 1597 cm^{-1} in Fig. 1c was assigned to the ring stretching mode of 44bpy. Appearance of this band at −0.8 V has been proved due to the effect of resonant excitation between electrode surface and adsorbed molecules, i.e., under the charge transfer condition.[43,48–50] Other bands at 1478 and 1550 cm^{-1} in Fig. 1d are corresponding to the ring stretching and in-plain bending

modes of 22bpy, respectively.[16,43,49] The orientation of molecular absorption is different for each other. Previous investigations using the infrared absorption, scanning tunneling microscope, or SERS have revealed that 44bpy molecules adsorb vertically to the plane of the benzene ring with the tilted orientation via the single nitrogen atom to the negatively polarized Au surface while 22bpy molecules are also adsorbed with the edge-on orientation via two nitrogen atoms of respective two benzene rings in the cis orientation at this potential region under both light illumination and dark conditions. [49–52] Our previous study about electrochemical SERS measurements for 22bpy and 44bpy molecules also confirmed each orientation under the full coverage condition.[16]

We have obtained time-series SERS spectra of each bpy molecule (not bi-analyte condition) as in the bottom of Fig. 1c and d. The concentrations of each molecule were 1 μM, corresponding to the condition for the unsaturated coverage of molecules at the metal surface.[48,53,54] The red and blue plots in bottom columns of Fig. 1c and d indicate the relative scattering intensities ratios at 1597 (44bpy: red) and 1478 (22bpy: blue) cm^{-1} estimated by dividing the given intensity at a specific time (I_t) by the initial intensity at 1 sec (I_{1s}) as the function of the laser illumination time (bottom column of the Fig. 1c and d). The original spectra are given in Fig. S2 and S3. As can be found in the original SERS spectra and plots, Raman spectra for both molecules showed the fluctuation behavior during laser illumination time of 60 sec. Because the SERS intensity directly reflects the number of molecules at the hot spot, the present intensity fluctuations would indicate the molecular hopping in/out at SERS hot spot due to the thermal equilibrium condition. It could be mentioned that under the present laser condition (λ_{ex} = 785 nm, incident intensity below 140 μW μm^{-2}), the plasmonic structure is relatively stable. We have revealed that the elevation of temperature by electron damping is less than 10 K under the present light intensity condition.[55] Therefore, it can be defined as that the present fluctuation of scattering intensity reflects the molecular hopping. In both molecular

cases, although the number of the molecules seems to be increased during observations, the plasmonic molecular trapping is not apparent because of the almost same intensity rations at the initial and final points. Finite-Difference Time-Domain (FDTD) calculations give an optical force value of 4.29 fN per single 44bpy molecule with edge-on orientation (α_{zz}) and optical potential of −0.07 k_BT at a 1 nm gap of Au bowtie structure under the present experimental condition (λ_{ex} = 785 nm with 140 μW μm^{-2}. The optical forces to 22bpy with the cis edge-on orientation (α_{zz}) can be calculated as 4.72 fN with edge-on orientation (details are given in Supporting Information). These values are relatively small compared to the threshold (0.1 pN) of the molecular trapping at room temprature.[24] Therefore, the present tendency in Fig. 1c and 1d would be reasonable. It should be noted that these estimations were based on the polarizability obtained from a simple isolated molecule model. In other words, we did not consider about the effect of the adsorption onto the metal surface as well as the interaction between molecules and metals to induce the charge transfer effect based on the resonant electronic excitation, leading to the increase of the polarizability. At the present dilute condition, the molecules have the less chance for the interaction because of the low coverage.[48] In addition, the previous effort revealed that the difference of theoretically estimated polarizabilities for both isolated and adsorbed molecules were less than 10%.[56] Therefore, our present estimation seems to be reasonable.

As the next step, time series SERS spectra have been obtained by using the different light intensity in the bi-analyte solution of 1 μM 44bpy and 1 μM 22bpy in 0.1 M $NaClO_4$ aq. under the constant potential at −0.8 V. Raman spectra were collected with the CCD detection time of 1 sec during 60 sec illumination corresponding to from bottom spectra to top ones in Fig. 2. In the bottom columns of figure, the time series changes in the Raman intensity at 1597 cm^{-1} (44bpy) and 1478 (22bpy) cm^{-1} are plotted as the function of the laser illumination time. For the discussion about the incident light intensity dependence, intensity plots have been

standardized by dividing scattering intensity with incident intensity based on the assumption that Stokes Raman intensities linearly increase with increasing the incident intensity.[57,58,] In the bi-analyte solution, the 22bpy is preferably adsorbed to the Au surface but, considering the present low concentration, the Au surface is not fully covered with 22bpy and slight amounts of 44bpy also exist at the surface.[16,48,51,53,59] It is important that the orientations for 22bpy and 44bpy were same as for the single component cases (Fig. 1). Interestingly, not only the increase of number of molecules with the time for the illumination, but also the selective increase of 22bpy were clearly observed under the relatively stronger light illumination. It is noted that such SERS intensity increments were not observed under the lower intensity than 35 μW μm^{-2}. Such molecular selective condensation could not be explained by simple thermal diffusion because these two isomers show almost same thermophoresis behavior, especially under the present concentration condition.[60,61] Even if thermophoresis effect contributed to trapping phenomena, the thermal force would be expected as relatively small since Solet coefficient depends on mainly molecular size.[62,63] Therefore, this SERS intensity increase would imply the changes in the number of molecules at the observation site induced by the light illumination. Note that observed molecule selectivity depending on the light intensity is characteristics to the case of the bi-analyte system. Considering this fact and the light intensity dependence, it can be expected that observed results would be correlated with the effect of the plasmonic field because the F_{opt} is linearly increasing depending on the incident light intensity (eq. 1).

With the aim of quantitative analyses of the molecular number changes, the histogram of the SERS intensities at the specific Raman band under different light intensity were shown as in Fig. 3. The x-axis in Fig. 3 represents the Raman intensity of the specific Raman band and the y-axis indicates that how many times the specific intensity were observed. In Fig. 3a and b, the Raman band intensities at 1478 cm^{-1} (22bpy: top) are dispersed at around 20 and 30 cps with the intensity of 35 and 70 μW μm^{-2}, respectively. On the other hand, in the case for

the relatively strong intensity with 140 μW μm^{-2} (Fig. 3c), the two dispersion centers were observed at around 10 and 45 cps corresponding to the initial and latter parts of observations (Fig. 2c). The number of molecule can be estimated from the Raman intensity ($I_{\omega_{Raman}}$) as described in the following equation:[64,65]

$$I_{\omega_{Raman}} = \mathrm{C} \times \mathrm{M} \times (\omega_0 - \omega_{Raman})^4 N_{sca} t_{det} I_{in} \left(\rho \alpha_{\rho\sigma} \sigma\right)^2 \quad \text{(eq. 2)}$$

where C is the constant defined by the cell condition, optical set up, and some physical constants while the M is the magnitude of plasmon enhanced electric field intensity determined by substrate.[66] The term of $\alpha_{\rho\sigma}$ is the scattering tensor which is the static at the present electrochemical potential.[67] All spectra were obtained with the same CCD detection time (t_{det}) of 1 sec under continuous exposure for 30 to120 sec. Since the incident intensity (I_{in}) has been kept constant during laser illumination, the N_{sca} can be given as the number of molecules at the hot spot. From the above calculations and the Lorentz fitting shown as the black lines, it was found that about 5 counts for each peak were equivalent to the signal from the single molecule. Thus, it allows us to evaluate that the number of 22bpy molecules verified from 4 to 9 as intensity changes from 35 to 140 μW μm^{-2}. At the same time, the slight increment of the number of 44bpy molecules at observation sites can be recognized from the same estimation (bottom panels). At the present experiments, we have observed the small size region with around 100 nm^2, which was estimated from the FDTD calculations, Previously documented results showed the respective surface coverage of 22bpy and 44bpy was less than 10% in 1 μM solution at room temperature under the dark condition.[48,53] Thus, considering the concentration, size of molecules, and the Langmuir adsorption isotherm, the number of molecules at 100 nm^2 region could be estimated as around 1 molecule, promised by the estimated number of increased molecules in experimental results. It is noteworthy that the standard deviations of the background intensity for each molecule normalized by the incident intensity have been taken into consideration at the present case (see in Table S1). From these quantitative estimations of

number of molecules at the hot spot, the occurrence of selective 22bpy condensations in the bi-analyte solution under the electrochemical potential control was successfully implied.

The spectral analyses of the molecule condensation during the long-time light exposure were conducted through two-dimensional time series SERS spectra under the illumination with distinct light intensities as in Fig. 4a, b, and c. As discussed above, the gradual increase of the scattering intensity, indicating the increment of the changes in the number of molecules at the hot spot, were confirmed in both bpy cases especially under the stronger light intensity condition. The increase of scattering intensity at 1478cm^{-1} is corresponding to the selectively condensation of 22bpy. In Fig. 4d, typical SERS spectra collected at 100 s with different laser intensity were depicted. In the case for 22bpy molecules, the spectrum shape was independent on the laser intensity while the Raman band for 44bpy at 1600 cm^{-1} became broaden with increasing light intensity. This broadening peak can be deconvoluted into two peaks, corresponding to 1608 cm^{-1} (brown area) and 1597 cm^{-1} (red area) assigned to ring stretching (C-C, C-N) modes.[68] The former and latter bands indicate the vertical and declined orientations of 44bpy against the negatively charged surface.[43,52,69]

Especially, the non-totally symmetric mode at 1597 cm^{-1} is the characteristics to the occurrence of the resonant charge transfer (CT) between the Fermi level of Au and molecules.[43,70–72] From Fig. 4d, it was found that the light illumination with the relatively strong intensity leads to the effective CT condition. According to the previous report, the α' of the molecule under the resonant condition is almost ten times larger than that with the non-resonant state, resulting in ten times higher efficiency of molecular trapping.[24] Taking above facts into considerations, it can be summarized that, when the distinct condensation of 22bpy occurs, the F_{opt} to 44bpy is enhanced up to ten times because of the CT state. In other words, 22bpy molecules which preferably absorbed to the negatively charged surface were condensed with the help by 44bpy molecules feeling much stronger F_{opt}. These facts would imply that the actual

F_{opt} applied to respective 22bpy and 44bpy molecules in the mixed solution could be higher than those estimated from the values of polarizability of isolated molecules (given above). Considering the characteristics to the bi-analyte condition and the spectrum analyses, the presence of the isomer molecules ant interaction between them must be the conceivable factors to modify the F_{opt}.

When the molecules interact each other, the domain like structure often forms. In the case for the bipyridine molecules, the relatively strong π-π stacking results in the formation of the molecular layer.[73,74] The well-defined molecular orientation kept by the electrochemical potential can accelerate such formation at interface.[51] It is known that the domain structures lead to the improvement of the α' compared to that of single molecule, leading to the relatively large trapping potential. [19,24,75,76] In our previous study, we have observed that the formation of the unique domain structures in the present bi-analyte solution could modulate the surface diffusion process especially under the CT state.[46] The similar domain like structure formation can be expected to occur during the condensation. Note that, because of the present dilute condition, the molecular interaction would be less at the initial stage of the light illumination. Thus, based on these facts, it can be assumed that such domain structure formation after the selective molecular condensation was assisted by the molecular interaction. In order to prove this assumption, we have done the repetitive long-time exposure experiment with dark interval. Because the surface diffusion of the domain structure is much suppressed under the thermal equilibrium condition, the repetitive light illumination with the dark interval enables us to vitalize the effect of the domain structures on the molecular condensation.

The upper parts of Fig. 5a show the two-dimensional SERS intensity collected by the four times continuous laser illumination for 60 seconds with the dark interval of 60 sec, which images is colored with respective intensity at each illumination. The electrochemical potential was kept at −0.8 V, enabling the resonant charge transfer. The black parts of figure are

corresponding to the dark condition. The bottom parts of Fig. 5a indicate the scattering intensities at 1478 (blue bars) and 1597 (red bars) cm^{-1}. The band intensities at 1608 cm^{-1} (brown bars) are also indicated at the opposite sides to them for the comparison of changing the adsorbed molecules under illumination. In the left column of Fig. 5a, corresponding to the first time illumination, 22bpy molecules seem to be selectively trapped, which is good agreement with above results. In the dark condition, the condensed 22bpy molecules formed by the light illuminations would be partially dispersed from hot spot and 44bpy molecules get the space. Thus, early parts in the second illumination, both 22bpy and 44bpy are few on the SERS hot spot as can be found in 2D image and intensity. On the other hands, in the latter parts of the second panel, the intensities for both molecules become gradually stronger than those in the first time illuminations, originating from the increments of the molecular interactions at the hot spot under the CT condition. At around 45 to 55 sec, the number of 22bpy at the hot spots rapidly increased, then both molecules are simultaneously condensed after that. This phenomenon would imply the formation of the relatively large domain structure consisting of 22bpy and 44bpy by the interaction between them after the condensation of 22bpy, leading to the efficient trapping. As the proof for the formation of the domain structure, the SERS intensities for both 22bpy and 44bpy are maintained at the biggening of the third time laser illumination even after dark interval. In the third and fourth illuminations, it was clearly vitalized that the repeated light and dark process gave father condensation. Especially for the 44bpy molecule, although the 44bpy is fluctuating, the intrinsic vibration of the 44bpy molecule (1597 cm^{-1}) excited under the CT resonance mainly appears in the condensed phase at fourth illumination comparing to before, leading to the suppression of the surface diffusion because of the large dipole and large polarizability as can be seen in the intensities plots. Incidentally, the fourth time illumination, although the number of molecules were dispersed, around 40 or 90 molecules were condensed at the hot spot in both cases of 22bpy and 44bpy

(see in Fig. S4). Therefore, from the investigations of Fig. 5a, it can be said that the molecular behavior in the bi-analyte solution is regulated by not only the effect of F_{opt} to each molecule but also the interaction between the molecules in the domain structures, resulting in the stable adsorption, and / or the polarizability changes under the CT resonance. This means that the unique molecular condensation was achieved by the synergistic influence of F_{opt} and attractive force between molecules at the electrified interface.

As the further analyses for the molecular behavior at the hot spot, the synchronous intensity correlations of the vibration modes were prepared as shown in Fig. 5b. This kind of synchronous correlation plot enables to visualize the molecular switching at the observation site because the red and blue areas correlated to intersection of vibration modes means positive and negative fluctuations, respectively.[49,77,78] Asynchronous analyses were also provided in Fig. S5. At the initial region, any cross-peaks at one of 44bpy and 22bpy vibrations did not appear and correlate there but the cross-peak at 1550 cm^{-1} of against 1478 cm^{-1} of 22bpy give sharp red spots. This implies that almost all 22bpy molecules are kept with a certain orientation during first illumination because all vibration mode intensities are increased / decreased at the same time. When the correlation between the charge transfer mode of 44bpy at 1597 cm^{-1} vs vibrational modes of 22bpy at 1478 cm^{-1} show relatively positive in the third column, this can be said as that both 44bpy with the declined orientation and cis oriented 22bpy were gradually condensed as in the same way. When we focus on the vibration mode of 44bpy at around 1600 cm^{-1}, in the fourth column of Fig. 5b, the red spot is widely split to 1597 cm^{-1} and 1608cm^{-1} because of the fluctuating the molecules. Hence, the correlation between around 1600 cm^{-1} and 1478 cm^{-1}, corresponding to 44bpy and 22bpy, shows negative behavior (blue spot). This is derived from the fact that each molecule alternately comes in and out the hot spot. It is important that, when the concentration of molecules is much higher (~ 1mM), such molecular hopping behavior is difficult to observed because the surface is fully covered by the

molecules.[16] These correlation plots strongly insist that the number of molecules at the surface reached almost saturated conditions even under the lower concentration of 1 μM. Although the optical potential could only retard the Brownian motion of the molecule during the illumination condition, it was clear that the molecular condensation states at the electrified Au surface would keep the effect of the laser illumination even after turning off the light due to the strong molecular interaction because of the formation of the domain structure. These phenomena would provide a new concentration equilibrium state or dissipative structure *via* light-matter interaction.

Consequently, we have proposed that it is possible to achieve the small size molecular trapping under the ambient condition especially under the bi-analyte and electrochemical conditions. The number of molecules achieved up to 90 times larger than that for the single component case as can be found from Fig. S4. For that, the interaction between the molecules is quite important. Considering the fact that the binding energy of π-π stacking in pyridine dimer reached the 32 and 16 kJ mol^{-1} for antiparallel and parallel configuration, respectively,[73,74] the control of the molecular orientation by the electrochemical potential control should be the key factor for the realization of the small size molecular trapping. As the proof of this point, we have achieved the clear molecular trapping behavior in the single component solution under the much higher concentration condition (1 mM) as shown in Fig. S6. This is because that, under such higher concentration condition, the metal surface is fully covered with the molecular, leading to the strong interaction with each other.[16,51]

The charge transfer process induced by the electrochemical potential scan between the metal and molecules also plays an important role within the domain structure to enhance the optical force. The 44bpy showing charge transfer resonant state can trigger the neighboring isomers to order more effectively by molecular interaction beyond the thermal isotherm under the specific electrochemical potential. By the accurate control of these factors, this plasmon

advanced molecular selective condensation can overcome the isothermal limitation and reveal the unrecognized molecular interactions.

CONCLUSIONS

Unique molecular condensation phenomena have been successfully observed in the bi-analyte solution under electrochemical potential control. As the effect of the optical force at the plasmonic field, the gradual increments of the molecules have been observed. It was found that the charge transfer resonance triggered by the electrochemical potential scan played important role for the molecular condensation. It has been also firstly revealed that the molecular interaction between the neighboring molecules affects to the additional contribution of the molecular selective condensation. Plasmon triggered molecular condensation is obviously overcome adsorption equilibrium defined by thermal isotherm. In other words, the plasmon-assisted molecular condensation under the ambient condition is established by present way. Moreover, curious behaviors are observed for binary mixture system as unique condensation phase, where much effectively break the physical limitation for molecular manipulation. We are sure that the above results provide the important information about the plasmonic optical trapping and, further, improve the possibility of the molecular manipulation technology for the application to the desirable chemical reaction control.

ASSOCIATED CONTENT

Supporting Information Available: <Systematic scheme of Raman measurement, FDTD modeling of Au dimer and optical force estimation, raw spectra of single component SERS, background deviation analysis, long-time histogram analysis of mixed solution, 2D

asynchronous correlation analysis, time series intensity plot of single component 1 mM solution. >

Notes

The authors declare no competing financial interests.

ACKNOWLEDGMENT

We appreciate discussion with Hajime Ishihara (Osaka University) and Keiji Sasaki (Hokkaido University). This work was partially supported by Grants-in-Aid for Scientific Research (Nos. JP18K14309 and JP18H05205) and Grants-in-Aid for JSPS Fellows (JP20J20967) from the Ministry of Education, Culture, Sports, Science, and Technology of Japan. Especially a lot of support by Scientific Research on Innovative Areas "Nano-Material Optical-Manipulation" (No. JP16H06506). Supports by the JST-Mirai Program Grant Number JPMJMI21EB, the Frontier Photonic Sciences Project of National Institutes of Natural Sciences (NINS) Grant Number 01213010, and the Photo-excitonix Project in Hokkaido University are also acknowledged.

REFERENCES

(1) Fröhlich, H. *Theory of Dielectrics: Dielectric Constant and Dielectric Loss*; Clarendon Press, 1949.

(2) Ashkin, A.; Dziedzic, J. M.; Bjorkholm, J. E.; Chu, S. Observation of a Single-Beam Gradient Force Optical Trap for Dielectric Particles. *Opt. Lett.* **1986**, *11* (5), 288–289.

(3) Alpeggiani, F.; D'Agostino, S.; Sanvitto, D.; Gerace, D. Visible Quantum Plasmonics from Metallic Nanodimers. *Sci. Rep.* **2016**, *6* (1), 34772.

(4) Dodson, S.; Haggui, M.; Bachelot, R.; Plain, J.; Li, S.; Xiong, Q. Optimizing Electromagnetic Hotspots in Plasmonic Bowtie Nanoantennae. *J. Phys. Chem. Lett.* **2013**, *4* (3), 496–501.

(5) Kolloch, A.; Geldhauser, T.; Ueno, K.; Misawa, H.; Boneberg, J.; Plech, A.; Leiderer, P. Femtosecond and Picosecond Near-Field Ablation of Gold Nanotriangles: Nanostructuring and Nanomelting. *Appl. Phys. A* **2011**, *104* (3), 793–799.

(6) Halas, N. J.; Lal, S.; Chang, W. S.; Link, S.; Nordlander, P. Plasmons in Strongly Coupled Metallic Nanostructures. *Chem. Rev.* **2011**, *111* (6), 3913–3961.

(7) Narang, P.; Sundararaman, R.; Atwater, H. A. Plasmonic Hot Carrier Dynamics in Solid-State and Chemical Systems for Energy Conversion. *Nanophotonics* **2016**, *5* (1), 96–111.

(8) George, J.; Chervy, T.; Shalabney, A.; Devaux, E.; Hiura, H.; Genet, C.; Ebbesen, T. W. Multiple Rabi Splittings under Ultrastrong Vibrational Coupling. *Phys. Rev. Lett.* **2016**, *117* (15), 1–10.

(9) Kale, M. J.; Avanesian, T.; Christopher, P. Direct Photocatalysis by Plasmonic Nanostructures. *ACS Catal.* **2014**, *4* (1), 116–128.

(10) Nishijima, Y.; Ueno, K.; Kotake, Y.; Murakoshi, K.; Inoue, H.; Misawa, H. Near-Infrared Plasmon-Assisted Water Oxidation. *J. Phys. Chem. Lett.* **2012**, *3* (10), 1248–1252.

(11) Konishi, T.; Kiguchi, M.; Takase, M.; Nagasawa, F.; Nabika, H.; Ikeda, K.; Uosaki, K.; Ueno, K.; Misawa, H.; Murakoshi, K. Single Molecule Dynamics at a Mechanically Controllable Break Junction in Solution at Room Temperature. *J. Am. Chem. Soc.* **2013**, *135* (3), 1009–1014.

(12) Zhang, J.; Zhou, R.; Minamimoto, H.; Yasuda, S.; Murakoshi, K. Nonzero Wavevector Excitation of Graphene by Localized Surface Plasmons. *Nano Lett.* **2019**, *19* (11), 7887–7894.

(13) Nagasawa, F.; Takase, M.; Murakoshi, K. Raman Enhancement via Polariton States Produced by Strong Coupling between a Localized Surface Plasmon and Dye Excitons at Metal Nanogaps. *J. Phys. Chem. Lett.* **2014**, *5* (1), 14–19.

(14) Kato, F.; Minamimoto, H.; Nagasawa, F.; Yamamoto, Y. S.; Itoh, T.; Murakoshi, K. Active Tuning of Strong Coupling States between Dye Excitons and Localized Surface Plasmons via Electrochemical Potential Control. *ACS Photonics* **2018**, *5* (3), 788–796.

(15) Minamimoto, H.; Kato, F.; Murakoshi, K. Surface-Enhanced Raman Scattering Probe for Molecules Strongly Coupled with Localized Surface Plasmon under Electrochemical Potential Control. *J. Raman Spectrosc.* **2021**, *52* (2), 431–438.

(16) Oyamada, N.; Minamimoto, H.; Murakoshi, K. In Situ Observation of Unique Bianalyte Molecular Behaviors at the Gap of a Single Metal Nanodimer Structure via Electrochemical Surface-Enhanced Raman Scattering Measurements. *J. Phys. Chem. C* **2019**, *123* (40), 24740–24745.

(17) Misawa, H.; Koshioka, M.; Sasaki, K.; Kitamura, N.; Masuhara, H. Three-dimensional Optical Trapping and Laser Ablation of a Single Polymer Latex Particle in Water. *J. Appl. Phys.* **1991**, *70* (7), 3829–3836.

(18) Yuyama, K. I.; Sugiyama, T.; Masuhara, H. Laser Trapping and Crystallization Dynamics of L-Phenylalanine at Solution Surface. *J. Phys. Chem. Lett.* **2013**, *4* (15), 2436–2440.

(19) Dienerowitz, M.; Mazilu, M.; Dholakia, K. Optical Manipulation of Nanoparticles: A Review. *J. Nanophotonics* **2008**, *2* (1), 021875.

(20) Vettenburg, T.; Dalgarno, H. I. C.; Nylk, J.; Coll-Lladó, C.; Ferrier, D. E. K.; Čižmár, T.; Gunn-Moore, F. J.; Dholakia, K. Light-Sheet Microscopy Using an Airy Beam. *Nat. Methods* **2014**, *11* (5), 541–544.

(21) Yan, Z.; Scherer, N. F. Optical Vortex Induced Rotation of Silver Nanowire. *J. Phys. Chem. Lett.* **2013**, *4* (17), 2937–2942.

(22) Osborne, M. A.; Balasubramanian, S.; Furey, W. S.; Klenerman, D. Optically Biased Diffusion of Single Molecules Studied by Confocal Fluorescence Microscopy. *J. Phys. Chem. B* **1998**, *102* (17), 3160–3167.

(23) Ashkin, A.; Dziedzic, J. M. Optical Trapping and Manipulation of Viruses and Bacteria. *Science* **1987**, *235* (4795), 1517–1520.

(24) Xu, H.; Käll, M. Surface-Plasmon-Enhanced Optical Forces in Silver Nanoaggregates. *Phys. Rev. Lett.* **2002**, *89* (24), 246802.

(25) Plonsey, R.; Collin, R. E. *Principles and Applications of Electromagnetic Fields*; McGraw-Hill, 1961.

(26) Grigorenko, A. N.; Roberts, N. W.; Dickinson, M. R.; Zhang, Y. Nanometric Optical Tweezers Based on Nanostructured Substrates. *Nat. Photonics* **2008**, *2* (6), 365–370.

(27) Daly, M.; Sergides, M.; Nic Chormaic, S. Optical Trapping and Manipulation of Micrometer and Submicrometer Particles. *Laser Photonics Rev.* **2015**, *9* (3), 309–329.

(28) Zhang, W.; Huang, L.; Santschi, C.; Martin, O. J. F. Trapping and Sensing 10 nm Metal Nanoparticles Using Plasmonic Dipole Antennas. *Nano Lett.* **2010**, *10* (3), 1006–1011.

(29) Urban, A. S.; Carretero-Palacios, S.; Lutich, A. A.; Lohmüller, T.; Feldmann, J.; Jäckel, F. Optical Trapping and Manipulation of Plasmonic Nanoparticles: Fundamentals, Applications, and Perspectives. *Nanoscale* **2014**, *6* (9), 4458.

(30) Berthelot, J.; Acimovic, S. S.; Juan, M. L.; Kreuzer, M. P.; Renger, J.; Quidant, R. Three-Dimensional Manipulation with Scanning near-Field Optical Nanotweezers. *Nat. Nanotechnol.* **2014**, *9* (4), 295–299.

(31) Chen, C.; Juan, M. L.; Li, Y.; Maes, G.; Borghs, G.; Van Dorpe, P.; Quidant, R. Enhanced Optical Trapping and Arrangement of Nano-Objects in a Plasmonic Nanocavity. *Nano Lett.* **2012**, *12* (1), 125–132.

(32) Pang, Y.; Gordon, R. Optical Trapping of a Single Protein. *Nano Lett.* **2012**, *12* (1), 402–406.

(33) Shoji, T.; Kitamura, N.; Tsuboi, Y. Resonant Excitation Effect on Optical Trapping of Myoglobin: The Important Role of a Heme Cofactor. *J. Phys. Chem. C* **2013**, *117* (20), 10691–10697.

(34) Pin, C.; Ishida, S.; Takahashi, G.; Sudo, K.; Fukaminato, T.; Sasaki, K. Trapping and Deposition of Dye–Molecule Nanoparticles in the Nanogap of a Plasmonic Antenna. *ACS Omega* **2018**, *3* (5), 4878–4883.

(35) Kitahama, Y.; Funaoka, M.; Ozaki, Y. Plasmon-Enhanced Optical Tweezers for Single Molecules on and near a Colloidal Silver Nanoaggregate. *J. Phys. Chem. C* **2019**, *123* (29), 18001–18006.

(36) Jensen, R. A.; Huang, I. C.; Chen, O.; Choy, J. T.; Bischof, T. S.; Lončar, M.; Bawendi, M. G. Optical Trapping and Two-Photon Excitation of Colloidal Quantum Dots Using Bowtie Apertures. *ACS Photonics* **2016**, *3* (3), 423–427.

(37) Xu, Z.; Crozier, K. B. All-Dielectric Nanotweezers for Trapping and Observation of a Single Quantum Dot. *Opt. Express* **2019**, *27* (4), 4034–4045.

(38) Djorović, A.; Meyer, M.; Darby, B. L.; Le Ru, E. C. Accurate Modeling of the Polarizability of Dyes for Electromagnetic Calculations. *ACS Omega* **2017**, *2* (5), 1804–1811.

(39) Le Ru, E. C.; Meyer, M.; Etchegoin, P. G. Proof of Single-Molecule Sensitivity in Surface Enhanced Raman Scattering (SERS) by Means of a Two-Analyte Technique. *J. Phys. Chem. B* **2006**, *110* (4), 1944–1948.

(40) Kneipp, K.; Kneipp, H.; Manoharan, R.; Itzkan, I.; Dasari, R. R.; Feld, M. S. Near-Infrared Surface-Enhanced Raman Scattering Can Detect Single Molecules and Observe "Hot" Vibrational Transitions. *J. Raman Spectrosc.* **1998**, *29* (8), 743–747.

(41) Nie, S. Probing Single Molecules and Single Nanoparticles by Surface-Enhanced Raman Scattering. *Science* **1997**, *275* (5303), 1102–1106.

(42) Dos Santos, D. P.; Temperini, M. L. A. A.; Brolo, A. G. Intensity Fluctuations in Single-Molecule Surface-Enhanced Raman Scattering. *Acc. Chem. Res.* **2019**, *52* (2), 456–464.

(43) Yonezawa, Y.; Minamimoto, H.; Nagasawa, F.; Takase, M.; Yasuda, S.; Murakoshi, K. In-Situ Electrochemical Surface-Enhanced Raman Scattering Observation of Molecules Accelerating the Hydrogen Evolution Reaction. *J. Electroanal. Chem.* **2017**, *800*, 7–12.

(44) Maruyama, Y.; Ishikawa, M.; Futamata, M. Thermal Activation of Blinking in SERS Signal. *J. Phys. Chem. B* **2004**, *108* (2), 673–678.

(45) Oikawa, S.; Minamimoto, H.; Murakoshi, K. Reversible Electrochemical Tuning of Optical Property of Single Au Nano-Bridged Structure via Electrochemical under Potential Deposition. *Chem. Lett.* **2017**, *46* (8), 1148–1150.

(46) Oyamada, N.; Minamimoto, H.; Wakisaka, Y.; Murakoshi, K. Determination of Molecular Orientation in Bi-Analyte Mono-Molecule Layer through Electrochemical Surface-Enhanced Raman Scattering Measurements. *Chem. Lett.* **2019**, *48* (8), 820–823.

(47) Archibong, E. F.; Thakkar, A. J. Polarizabilities of Aromatic Six-Membered Rings: Azines and 'Inorganic Benzenes.' *Mol. Phys.* **1994**, *81* (3), 557–567.

(48) Uosaki, K.; Allen, H.; Hill, O. Absorption Behaviour of 4,4′-Bipyridyl at a Gold/Water Interface and Its Role in the Electron Transfer Reaction between Cytochrome c and a Gold Electrode. *J. Electroanal. Chem. Interf. Electrochem.* **1981**, *122*, 321–326.

(49) Butcher, D. P.; Boulos, S. P.; Murphy, C. J.; Ambrosio, R. C.; Gewirth, A. A. Face-Dependent Shell-Isolated Nanoparticle Enhanced Raman Spectroscopy of 2,2′-Bipyridine on Au(100) and Au(111). *J. Phys. Chem. C* **2012**, *116* (8), 5128–5140.

(50) Brolo, A. G. G.; Jiang, Z.; Irish, D. E. E. The Orientation of 2,2'-Bipyridine Adsorbed at a SERS-Active Au(1 1 1) Electrode Surface. *J. Electroanal. Chem.* **2003**, *547* (2), 163–172.

(51) Cunha, F.; Tao, N. J.; Wang, X. W.; Jin, Q.; Duong, B.; D'Agnese, J. Potential-Induced Phase Transitions in 2,2'-Bipyridine and 4,4'-Bipyridine Monolayers on Au(111) Studied by in Situ Scanning Tunneling Microscopy and Atomic Force Microscopy. *Langmuir* **1996**, *12* (26), 6410–6418.

(52) Wandlowski, T.; Ataka, K.; Mayer, D. In Situ Infrared Study of 4,4'-Bipyridine Adsorption on Thin Gold Films. *Langmuir* **2002**, *18* (11), 4331–4341.

(53) Yang, D.; Bizzotto, D.; Lipkowski, J.; Pettinger, B.; Mirwald, S. Electrochemical and Second Harmonic Generation Studies of 2,2'-Bipyridine Adsorption at the Au(111) Electrode Surface. *J. Phys. Chem.* **1994**, *98* (28), 7083–7089.

(54) Chaffins, S. A.; Gui, J. Y.; Kahn, B. E.; Lin, C. H.; Lu, F.; Salaita, G. N.; Stern, D. A.; Zapien, D. C.; Hubbard, A. T.; Elliott, C. M. Adsorption of Bipyridyls and Structurally Related Compounds at Platinum(111) Electrodes: Studies by Vibrational Spectroscopy (EELS), Auger Spectroscopy, and Electrochemistry. *Langmuir* **1990**, *6* (5), 957–970.

(55) Takase, M.; Nabika, H.; Hoshina, S.; Nara, M.; Komeda, K.; Shito, R.; Yasuda, S.; Murakoshi, K. Local Thermal Elevation Probing of Metal Nanostructures during Laser Illumination Utilizing Surface-Enhanced Raman Scattering from a Single-Walled Carbon Nanotube. *Phys. Chem. Chem. Phys.* **2013**, *15* (12), 4270–4274.

(56) Deutsch, D.; Natan, A.; Shapira, Y.; Kronik, L. Electrostatic Properties of Adsorbed Polar Molecules: Opposite Behavior of a Single Molecule and a Molecular Monolayer. *J. Am. Chem. Soc.* **2007**, *129* (10), 2989–2997.

(57) Kneipp, K.; Kneipp, H. SERS Signals at the Anti Stokes Side of the Excitation Laser in Extremely High Local Optical Fields of Silver and Gold Nanoclusters. *Faraday Discuss.* **2006**, *132*, 27–33.

(58) Lombardi, A.; Schmidt, M. K.; Weller, L.; Deacon, W. M.; Benz, F.; de Nijs, B.; Aizpurua, J.; Baumberg, J. J. Pulsed Molecular Optomechanics in Plasmonic Nanocavities: From Nonlinear Vibrational Instabilities to Bond-Breaking. *Phys. Rev. X* **2018**, *8* (1), 011016.

(59) Mayer, D.; Dretschkow, T.; Ataka, K.; Wandlowski, T. Structural Transitions in 4,4′-Bipyridine Adlayers on Au(111) - An Electrochemical and in-Situ STM-Study. *J. Electroanal. Chem.* **2002**, *524–525*, 20–35.

(60) Kumar, P.; Goswami, D. Importance of Molecular Structure on the Thermophoresis of Binary Mixtures. *J. Phys. Chem. B* **2014**, *118* (51), 14852–14859.

(61) Polyakov, P.; Rossinsky, E.; Wiegand, S. Study of the Soret Effect in Hydrocarbon Chain/Aromatic Compound Mixtures. *J Phys. Chem. B* **2009**, *113* (40), 13308–13312.

(62) Braibanti, M.; Vigolo, D.; Piazza, R. Does Thermophoretic Mobility Depend on Particle Size? *Phys. Rev. Lett.* **2008**, *100* (10), 1–4.

(63) Braun, D.; Libchaber, A. Trapping of DNA by Thermophoretic Depletion and Convection. *Phys. Rev. Lett.* **2002**, *89* (18), 2–5.

(64) Albrecht, A. C. On the Theory of Raman Intensities. *J. Chem. Phys.* **1961**, *34* (5), 1476–1484.

(65) Kneipp, K.; Kneipp, H.; Manoharan, R.; Itzkan, I.; Dasari, R. R.; Feld, M. S. Surface-Enhanced Raman Scattering (SERS)-a New Tool for Single Molecule Detection and Identification. *Bioimaging* **1998**, *6* (2), 104–110.

(66) Le Ru, E. C.; Etchegoin, P. G. Rigorous Justification of the $|E|^4$ Enhancement Factor in Surface Enhanced Raman Spectroscopy. *Chem. Phys. Lett.* **2006**, *423* (1–3), 63–66.

(67) Jiang, S.; Zhang, Y.; Zhang, R.; Hu, C.; Liao, M.; Luo, Y.; Yang, J.; Dong, Z.; Hou, J. G. Distinguishing Adjacent Molecules on a Surface Using Plasmon-Enhanced Raman Scattering. *Nat. Nanotechnol.* **2015**, *10* (10), 865–869.

(68) Suzuki, M.; Niidome, Y.; Yamada, S. Adsorption Characteristics of 4,4′-Bipyridine Molecules on Gold Nanosphere Films Studied by Surface-Enhanced Raman Scattering. *Thin Solid Films* **2006**, *496* (2), 740–747.

(69) Rzeźnicka, I. I.; Horino, H.; Kikkawa, N.; Sakaguchi, S.; Morita, A.; Takahashi, S.; Komeda, T.; Fukumura, H.; Yamada, T.; Kawai, M. Tip-Enhanced Raman Spectroscopy of 4,4′-Bipyridine and 4,4′-Bipyridine N,N'-Dioxide Adsorbed on Gold Thin Films. *Surf. Sci.* **2013**, *617*, 1–9.

(70) Sprague-Klein, E. A.; McAnally, M. O.; Zhdanov, D. V.; Zrimsek, A. B.; Apkarian, V. A.; Seideman, T.; Schatz, G. C.; Van Duyne, R. P. Observation of Single Molecule Plasmon-Driven Electron Transfer in Isotopically Edited 4,4′-Bipyridine Gold Nanosphere Oligomers. *J. Am. Chem. Soc.* **2017**, *139* (42), 15212–15221.

(71) Sprague-Klein, E. A.; Ho-Wu, R.; Nguyen, D.; Coste, S. C.; Wu, Y.; McMahon, J. J.; Seideman, T.; Schatz, G. C.; Van Duyne, R. P. Modulating the Electron Affinity of Small Bipyridyl Molecules on Single Gold Nanoparticles for Plasmon-Driven Electron Transfer. *J. Phys. Chem. C* **2021**, *125* (40), 22142–22153.

(72) Prez-Jimnez, Á. J.; Sancho-García, J. C.; Prez-Jordá, J. M. Torsional Potential of 4, 4′ -Bipyridine: Ab Initio Analysis of Dispersion and Vibrational Effects. *J. Chem. Phys.* **2005**, *123* (13), 1–10.

(73) Mishra, B. K.; Sathyamurthy, N. π-π Interaction in Pyridine. *J. Phys. Chem. A* **2005**, *109* (1), 6–8.

(74) Hohenstein, E. G.; Sherrill, C. D. Effects of Heteroatoms on Aromatic π-π Interactions: Benzene-Pyridine and Pyridine Dimer. *J. Phys. Chem. A* **2009**, *113* (5), 878–886.

(75) Ghanty, T. K.; Ghosh, S. K. Correlation between Hardness, Polarizability, and Size of Atoms, Molecules, and Clusters. *J. Phys. Chem.* **1993**, *97* (19), 4951–4953.

(76) Wang, S.-F. F.; Yuyama, K. I.; Sugiyama, T.; Masuhara, H. Reflection Microspectroscopic Study of Laser Trapping Assembling of Polystyrene Nanoparticles at Air/Solution Interface. *J. Phys. Chem. C* **2016**, *120* (29), 15578–15585.

(77) Noda, I.; Ozaki, Y. *Two-Dimensional Correlation Spectroscopy - Applications in Vibrational and Optical Spectroscopy*; John Wiley & Sons, Ltd, 2004.

(78) Nagasaki, Y.; Yoshihara, T.; Ozaki, Y. Polarized Infrared Spectroscopic Study on Hindered Rotation around the Molecular Axis in the Smectic-C Phase of a Ferroelectric Liquid Crystal with a Naphthalene Ring. Application of Two-Dimensional Correlation Spectroscopy to Polarization Angle-Dependent. *J. Phys. Chem. B* **2000**, *104* (13), 2846–2852.

Figures

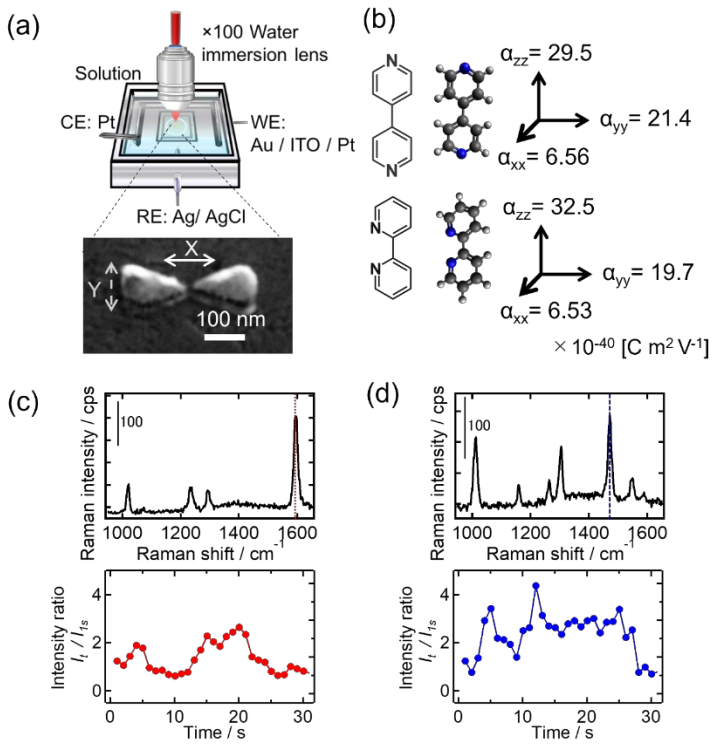

Figure 1 | (a) Schematic illustration of electrochemical SERS measurement system. The working, counter, and reference electrodes were Au bowtie / Ti / ITO, Pt plate, and Ag / AgCl, respectively. The electrolyte was 0.1 M $NaClO_4$. (b) Target molecules of 4,4'-bipyridine and 2,2'-bipyridine are shown with the values of static polarizability estimated from the density function theory by gaussian16, B3LYP, 6-31g(d,p)). Typical SERS spectra from (c) 1 μM 44bpy in 0.1 M $NaClO_4$ aq. and (d) 1 μM 22bpy in 0.1 M $NaClO_4$ aq. obtained at –0.8 V in upper panels. The laser intensity was set to 140 μW μm^{-2}. Raman scattering intensity change in time were plotted using the intrinsic vibration modes (c) for 44bpy: 1597 cm^{-1} (a red line) and (d) for 22bpy: 1478 cm^{-1} (a blue line) in lower panels.

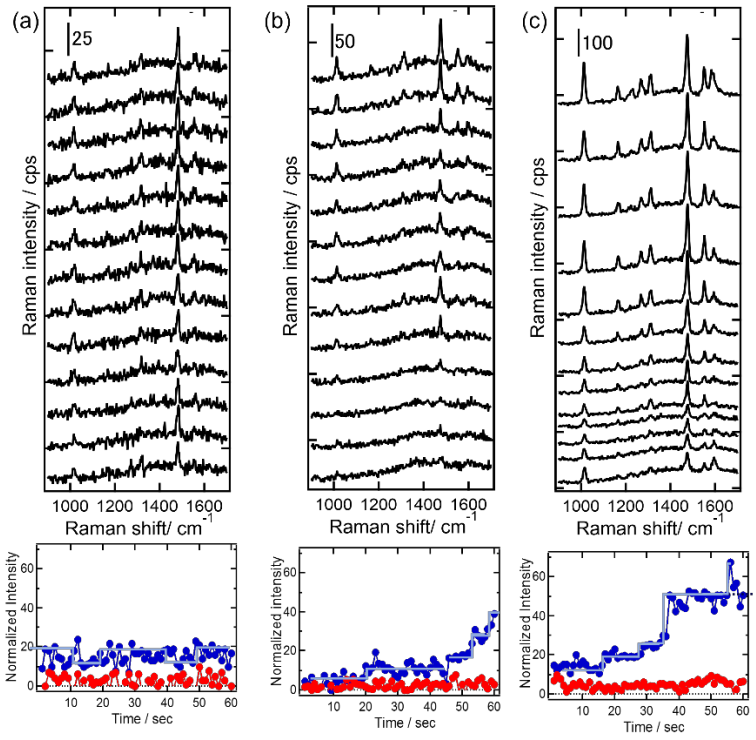

Figure 2 | Time series spectra of 1 μM 44bpy and 1 μM 22bpy in 0.1 M $NaClO_4$ aq. obtained in each laser illumination time of 1 s during 60sec from bottom to top. The electrode potential was set to –0.8 V vs. Ag / AgCl. The incident intensity for each were (a) 35, (b) 70, and (c) 140 μW μm^{-2}. Bottom inset plots for 44bpy at 1597 cm^{-1}(red line) and 22bpy at 1478 cm^{-1} extracted from these spectra with standardization by incident laser intensity.

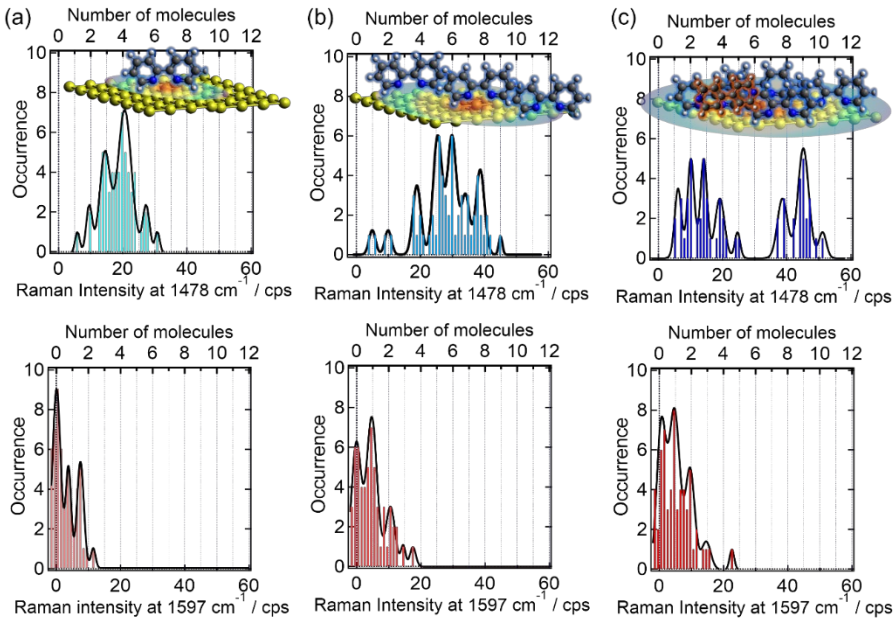

Figure 3 | Intensity histograms are estimated from time series SERS spectra of 1 μM 44bpy and 1 μM 22bpy in 0.1 M $NaClO_4$ aq. at –0.8 V with schematic picture of number of bpys. The blue and red bars are corresponding to the normalized peak intensity at 1597 cm^{-1} (44bpy; bottom panels) and 1478 cm^{-1} (22bpy; top panels), respectively. Panels are arranged in order of incident intensity: (a) 35, (b) 70, and (c) 140 μW $μm^{-2}$, from left to right. The black lines show intensity dispersion plotted with Lorentz fitting.

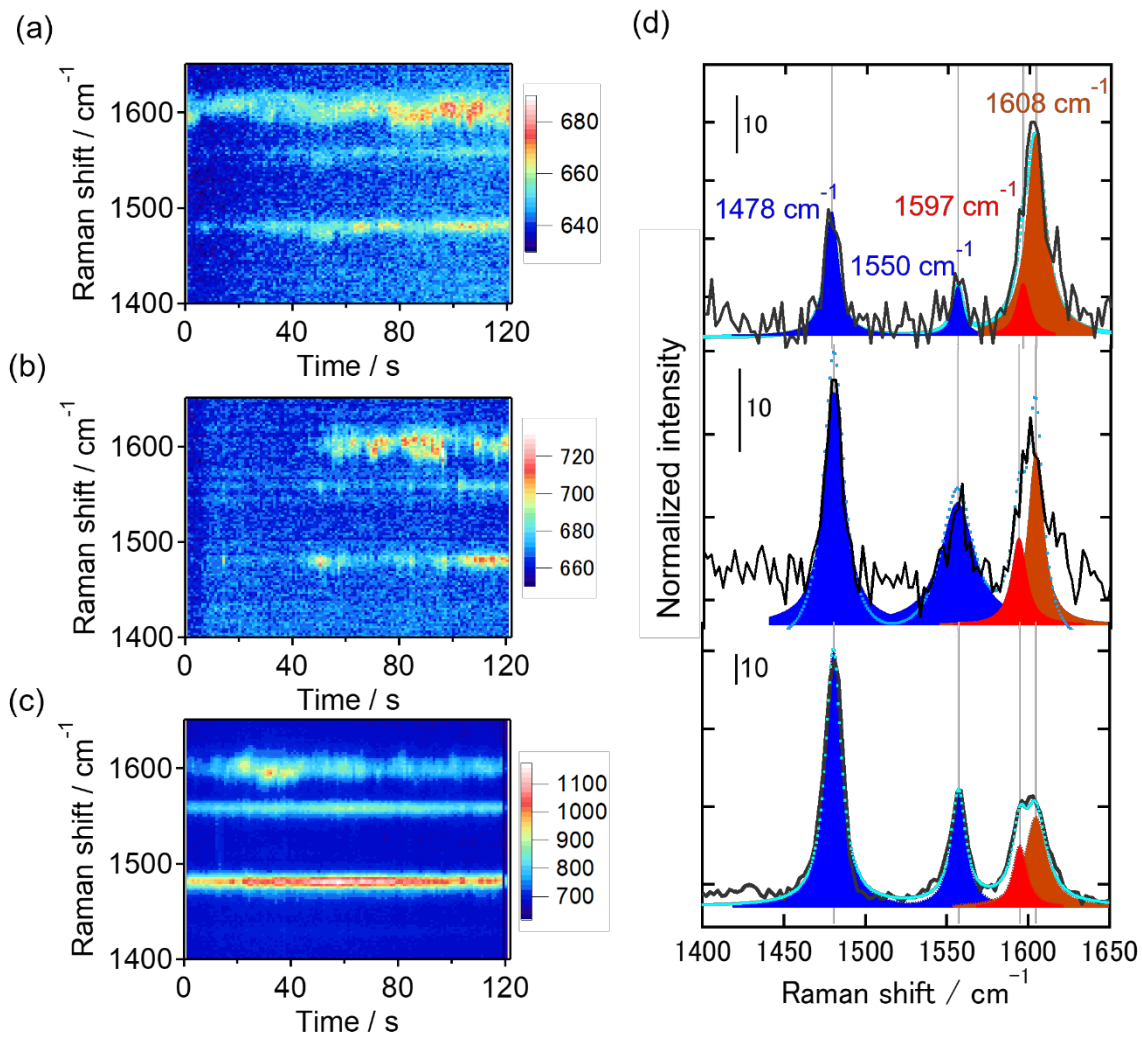

Figure 4 | 2D-image of time series SERS spectra of 1 μM 44bpy and 1 μM 22bpy in 0.1M $NaClO_4$ aq. collected at −0.8 V. The incident laser intensities were (a) 35, (b) 70, and (c) 140 μW μm^{-2}, respectively. (d) Normalized SERS spectra by incident laser intensity collected at laser illumination time of 100 sec. Fitting peaks at 1608 cm^{-1} and 1597 cm^{-1} are represented as brown and red areas. The fitting peaks at 1478 cm^{-1} and 1550 cm^{-1} (22bpy) are shown as blue. Light blue dots show total fitting area of these peaks.

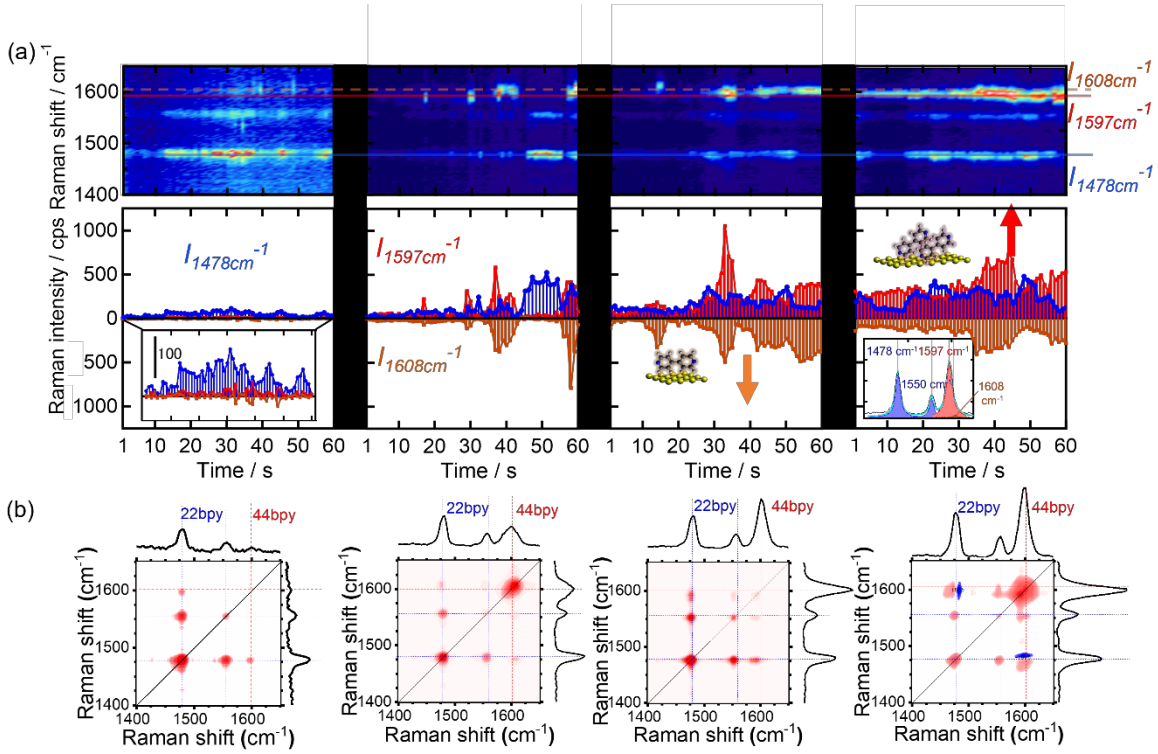

Figure 5 | (a) 2D-image of time series SERS spectra of 1 μM 44bpy and 1 μM 22bpy in 0.1 M $NaClO_4$ aq. at –0.8 V. Second panels show the change in the peak intensity at 1597 cm^{-1} (red), 1608 cm^{-1} (brown), and 1478 cm^{-1} (blue). The black areas correspond to the dark condition of 60 sec. The laser intensity was 140 μW $μm^{-2}$. Inset pictures are the schematic illustration of adsorption configuration of 44bpy and 22bpy. Inset SERS spectrum obtained at 50 sec of fourth illumination with fitting results. (b) 2D-syncronous plots with time average spectra in each axis. The red and blue spots show the positive and negative correlations, respectively.

TOC Graphic